DOI: 10.1002/adma.200703097

Simultaneous Use of Small- and Wide-Angle X-ray Techniques to Analyze Nanometerscale Phase Separation in Polymer Heterojunction Solar Cells**

By *Mao-Yuan Chiu, U-Ser Jeng, Chiu-Hun Su, Keng S. Liang,* and *Kung-Hwa Wei**

The development of conjugated polymers for use in organic optoelectronic devices has been an area of extensive investigation. Heterojunction polymer solar cells have been reported utilizing poly(*p*-phenylenevinylene) derivatives,[1] poly (3-alkylthiophene),[2] or low-bandgap polymers[3] as donors and fullerene derivatives as acceptors. Notably, poly(3-hexylthiophene)/[6,6]-phenyl-C_{61}-butyric acid methyl ester (P3HT/PCBM) bulk heterojunctions display power conversion efficiencies of up ca. 5%.[4] The improved power conversion efficiencies of these devices results from the use of thermal annealing[4a] and solvent annealing[4b] processes, which enhance the film morphology relative to that of the as-cast film. The resulting improvement in performance of these systems have been attributed to (i) self-organization of P3HT into a crystalline structure exhibiting enhanced absorption and high hole mobility/transport, and (ii) diffusion of PCBM molecules into PCBM-rich clusters to form large PCBM clusters. The nanostructured phase separation of P3HT/PCBM creates percolated pathways for transporting the holes and electrons to their respective electrodes. Therefore, the performance of these heterojunction solar cells depends critically on the morphology of their active layers.

Grazing-incidence X-ray diffraction (GIXRD) has been used previously to establish the dimensions of P3HT crystallites in P3HT/PCBM bulk heterojunction polymer solar cells;[5] morphological studies have also been undertaken using transmission electron microscopy (TEM) and electron diffraction.[6] The morphology of P3HT/PCBM bulk heterojunction solar cells after solvent annealing can also be analyzed using atomic force microscopy (AFM),[7] and scanning transmission X-ray microscopy (STXM)[8] has been applied to study the phase separation of PCBM on the order of several hundred nanometers, with a resolution limit of several tens of nanometers. These analytical tools, however, provide only a local view of the morphology; they cannot represent the full morphology of the active layer in the devices.

Small-angle X-ray scattering (SAXS), which utilizes the elastic scattering of X-rays to probe nanostructures having sizes ranging from 1 to 100 nm, provides statistically averaged morphologies of analyzed samples.[9] For polymer/fullerene bulk heterojunction solar cells, SAXS can provide global information regarding the internal structure of the dispersion of fullerene units within the polymer matrix much more effectively than can TEM or the other analysis techniques. In this present study, we simultaneously applied grazing-incidence small-angle X-ray scattering (GISAXS) and wide-angle X-ray diffraction (GIWAXD) to study the morphology of P3HT/PCBM bulk heterojunction solar cells after their thermal annealing. Utilizing this approach, we could therefore elucidate the relationship between the relative length scales of the PCBM clusters and P3HT crystallites and the devices' performance.

Figure 1a displays the GIWAXD profiles of several P3HT/PCBM films. After annealing the P3HT/PCBM film at 150 °C for 15 min, a strong peak appeared representing the (100) reflections of the P3HT lamella layer structure along with two small peaks contributed by the (300) and (400) or (010) plane reflections of the P3HT lamella structure.[10]

The sizes of the P3HT crystallites at (100) reflection (D_{100}) can be obtained using Scherrer's relation:[5,11]

$$D_{\mathrm{hkl}} = \frac{0.9\lambda}{\beta_{\mathrm{hkl}} \cos\theta} \quad (1)$$

where D_{hkl} is the apparent crystallite size along the [*hkl*] direction and β_{hkl} is the full width at half maximum of an (*hkl*) diffraction (in radians). The P3HT crystallites dramatically increased in size – from 9.6 nm in the as-cast film to 18.0 nm – after annealing at 100 °C for 15 min. This phenomenon can be explained by considering that the glass transition temperature in regioregular poly(3-alkylthiophene) is ca. 100 °C.[12] Table 1 lists the values of D_{100} for the P3HT crystallites obtained after annealing at various temperatures.

In Figure 1a, in the low-Q range (ca. 0.006 $\mathrm{Å}^{-1}$) of the GISAXS curves for the as-cast film, we observe a small scattering peak that is possibly attributable to the presence of PCBM in P3HT. For confirming this scattering peak, we have carried out control experiments by measuring GISAXS for both the pure P3HT and the P3HT/PCBM thin films

[*] Prof. K.-H. Wei, M.-Y. Chiu
Department of Materials Science and Engineering
National Chiao Tung University
1001 Ta Hsueh Road, Hsinchu 30050, Taiwan (ROC)
E-mail: khwei@mail.nctu.edu.tw
Dr. U.-S. Jeng, Dr. C.-H. Su, Dr. K. S. Liang
National Synchrotron Radiation Research Center
101 Hsin-Ann Road, Science-Based Industrial Park,
Hsinchu 30077, Taiwan (ROC)

[**] We thank the National Science Council of Taiwan for funding (NSC 96-2120-M-009-005). Supporting Information is available online from Wiley InterScience or from the authors.

 © 2008 WILEY-VCH Verlag GmbH & Co. KGaA, Weinheim

ADVANCED MATERIALS

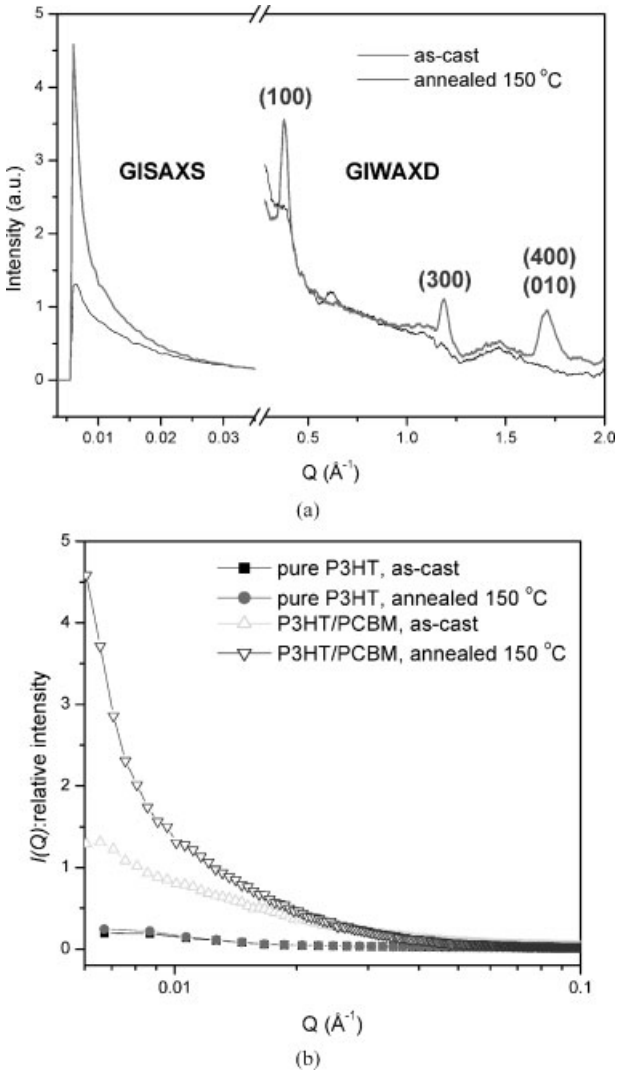

Figure 1. a) GISAXS/GIWAXD curves of as-cast and annealed (150 °C, 15 min) P3HT/PCBM films (not to scale). b) GISAXS curves of as-cast and annealed (150 °C, 15 min) P3HT and P3HT/PCBM thin films.

(ca. 100 nm thickness; on Si substrate). Figure 1b shows that the annealing at 150 °C for 15 min does not affect the low-Q intensity of the GISAXS profile of the P3HT film, indicating that even if there is local phase separation inside the P3HT film, it does not contribute much to the intensity change in the low-Q region. Moreover, the GISAXS intensity of the as-cast or annealed P3HT/PCBM thin film is much larger than that of the as-cast or annealed pure P3HT thin film, probably due to the large electron density difference between PCBM and P3HT (0.7 versus 0.4 $e^- Å^{-3}$). Therefore, the GISAXS features in the low-Q region of P3HT/PCBM thin film are clearly dominated by PCBM, and we attribute the large GISAXS intensity change in the P3HT/PCBM thin film after annealing at 150 °C for 15 min to a significant growth of the PCBM aggregates. The PCBM scattering intensity increased dramatically as a result of the PCBM molecules diffusing out of the P3HT matrix and forming larger PCBM clusters.[14]

Table 1. Values of R_g and D_{100} for PCBM cluster aggregates and P3HT crystallites obtained after annealing for 15 min at various temperatures.

Annealing temperature	R_g of PCBM [a] [nm]	Number of PCBM molecules [b]	D_{100} of P3HT [c] [nm]
As-cast	15 ± 2	10640	9.6
100 °C	16 ± 2	12320	18.0
120 °C	16 ± 2	14168	17.7
150 °C	23 ± 3	39608	16.0

[a] Determined using Guinier approximations to obtain the average value of R_g in the low-Q range. [b] Calculation by R_g of fullerenes for 0.38 nm, assuming a cubic lattice model for PCBM molecules (see Ref. [13]). [c] Determined using Scherrer's equation.

Figure 2 displays the morphologies of P3HT/PCBM thin films as determined through phase-contrast AFM measurements. Phase separation was more apparent – with domain sizes ranging from between 30 to 60 nm – for the sample that had experienced annealing at 150 °C for 15 min relative to that of the as-cast film. These images are consistent with the results obtained from the simultaneous GISAXS/GIWAXD analyses.

The radius of gyration (R_g) of a PCBM cluster can be determined from the scattering peak intensity using the Guinier approximation (Equation 2):

$$I(Q) = I(0)\exp\left(-\frac{Q^2 R_g^{\,2}}{3}\right) \quad (2)$$

where $I(Q)$ is the scattering intensity, $I(0)$ is the zero-angle scattering intensity, Q is defined as $4\pi\sin(\theta/2)/\lambda$ in terms of the scattering angle θ and the wavelength λ, and R_g is the radius of gyration of the PCBM clusters. Figure 3 presents plots of $\ln I(Q)$ versus Q^2 that were fit using Equation 2 (solid lines) in the low-Q range (0.006–0.012 $Å^{-1}$).[15] The values of R_g can be extracted from the slopes ($-R_g^{\,2}/3$) of the fitted lines. We fitted each set of data with two slopes for two R_g values that were then used to give an averaged R_g and the spread of R_g for the aggregation size of PCBM. Table 1 lists these values for the PCBM clusters obtained under various annealing conditions. After annealing at 100 and 120 °C, the values of R_g of the PCBM clusters increased marginally to (16 ± 2) nm from (15 ± 2) nm in the as-cast film. After annealing at 150 °C for 15 min, R_g increased dramatically to (23 ± 3) nm. Thus, it appears that large-scale diffusion of PCBM molecules into the P3HT matrix to form aggregates occurred only at temperatures at or above 150 °C. The mean diameter of the PCBM clusters obtained after annealing at 150 °C for 15 min was (60 ± 20) nm, as deduced from the value of R_g, assuming that the PCBM clusters were spherical.[16] This result is consistent with those obtained from TEM studies.[6]

Table 2 summarizes the current density–voltage characteristics of the P3HT/PCBM devices under illumination with respect to their annealing temperatures. Under 1 equivalent sun intensity (100 mW cm^{-2}), the power conversion efficiency (η) from our as-cast device was 0.53%, with values of J_{sc}, V_{oc}, and FF of 4.0 mA cm^{-2}, 0.38 V, and 35%, respectively. After annealing at 100 °C for 15 min, the value of η became 1.6%. We

© 2008 WILEY-VCH Verlag GmbH & Co. KGaA, Weinheim

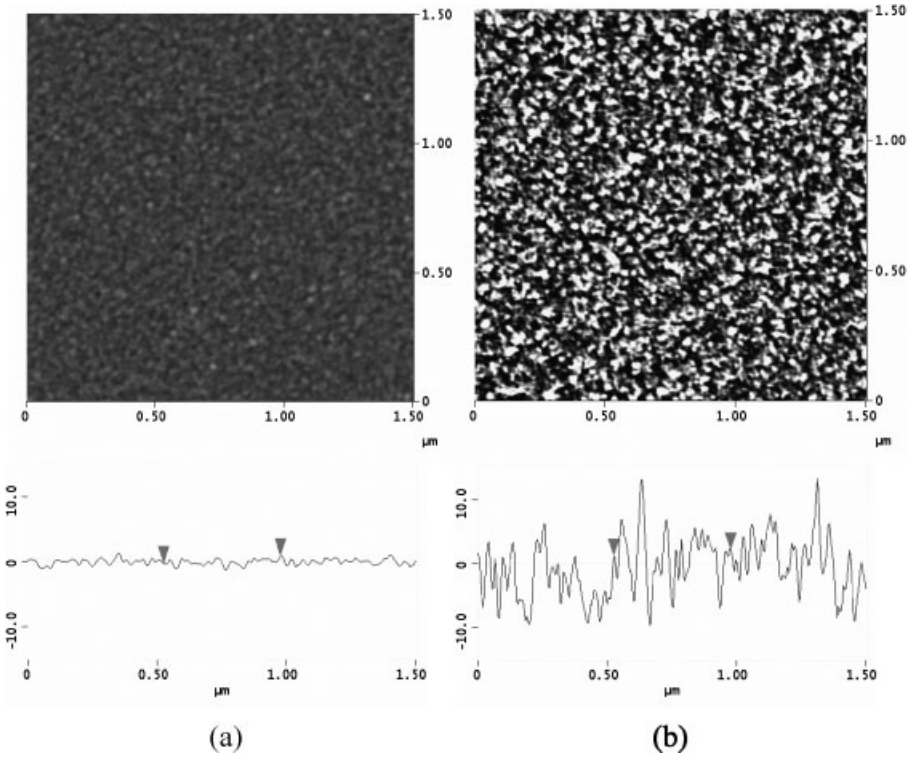

Figure 2. Phase-contrast AFM images of a) as-cast and b) annealed (150 °C, 15 min) P3HT/PCBM films.

attribute this increase in η to the growth of the P3HT crystallites, which increased to 18.0 nm from 9.6 nm after annealing, since the hole mobility increased upon increasing the size of the P3HT crystallites,[17] as evidenced by the current density increasing from 4.0 to 7.7 mA cm^{-2}. Furthermore, the change in the morphology of P3HT/PCBM film results in increased carrier delocalization.[18]

Annealing the P3HT/PCBM blend at 120 °C for 15 min, increased the value of η to 3.0%; we believe this behavior resulted from an increase in the number of P3HT crystallites, even though the average crystallite size remained about the same as that in the sample annealed at 100 °C (cf. stronger (100) peak in Fig. S1). The sizes of the PCBM clusters remained virtually unchanged when the annealing of P3HT/PCBM was performed at either 100 or 120 °C for 15 min. Annealing for 15 min at 150 °C, however, led to a dramatic increase in the value of R_g of the PCBM cluster aggregates to (23 ± 3) nm; accordingly, the η increased to 4.0%, with values of J_{sc}, V_{oc}, and FF of 9.9 mA cm^{-2}, 0.63 V, and 63%, respectively. In this case, the P3HT crystallite size reduced slightly relative to that for the sample annealed at 120 °C, whereas the absolute intensity of the (100) reflection remained roughly the same. Therefore, we interpret the increase in J_{sc} as resulting from larger PCBM clusters forming better pathways for electron transport. Hence, different mechanisms dominate the development of the P3HT/PCBM blend morphology at different temperatures. At the glass transition temperature (100 °C), increased planar stacking of P3HT chains occurred, thereby increasing the P3HT/PCBM crystallite size but not affecting the cluster size of the PCBM molecules. At 150 °C, the PCBM molecules diffused to form large clusters; therefore, phase separation of P3HT and PCBM occurred to provide improved continuous pathways for the holes and electrons. Figure 4 illustrates the morphologies of the as-cast and optimized devices.

Figure 5 displays the relative length scales of the P3HT crystallites and the radii of gyration of the PCBM clusters. The

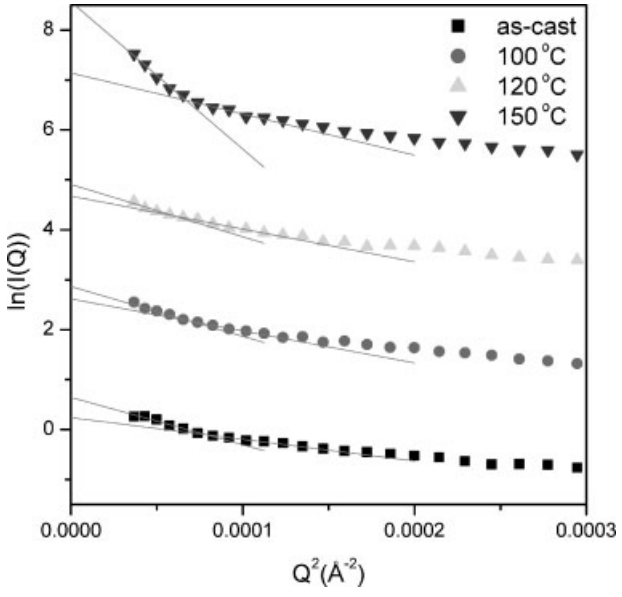

Figure 3. Plots of ln $I(Q)$ veruss Q^2 for P3HT/PCBM films annealed at various temperatures, fitted using the Guinier approximation (solid lines).

Table 2. Comparison of the P3HT crystal size, PCBM cluster size, and device electronic parameters at different annealed temperature for 15 min.

	D_{100} of P3HT [nm]	R_g of PCBM [nm]	J_{sc}[a] [mA cm^{-2}]	V_{oc}[b] [V]	FF[c] [%]	η[d] [%]
As-cast	9.6	15 ± 2	4.0	0.38	35	0.53
100 °C	18.0	16 ± 2	7.7	0.41	52	1.6
120 °C	17.7	16 ± 2	8.7	0.59	58	3.0
150 °C	16.0	23 ± 3	9.9	0.63	63	4.0

[a] Short-circuit current density. [b] Open-circuit voltage. [c] Filling factor. [d] Power-conversion efficiency.

 © 2008 WILEY-VCH Verlag GmbH & Co. KGaA, Weinheim

ADVANCED MATERIALS

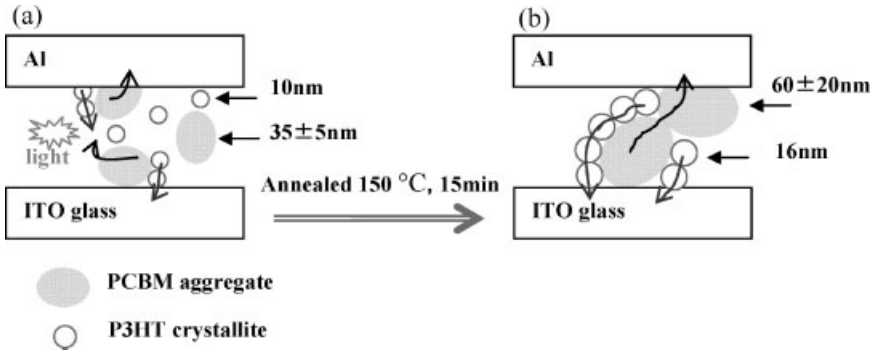

Figure 4. Schematic representation of P3HT/PCBM blends as active layers (ca. 100 nm) in solar cell devices. a) Non-annealed devices: holes and electrons recombine as a result of percolation. b) After annealing the devices at 150 °C for 15 min, the holes and electrons experience a good percolated network for their passage to the ITO and Al electrodes, respectively.

value of the corresponding lattice constant, d_{100}, can be calculated using Bragg's law ($n\lambda = 2d\sin\theta$ at $2\theta = 5.3^\circ$)[11] to be 1.67 nm. From Scherrer's relation, the value of D_{100} is equal to md_{100}, where m is the number of layers in the P3HT lamellar structure. For the device exhibiting the optimal performance (annealing temperature, 150 °C; P3HT:PCBM blend weight ratio, 1:0.8), each P3HT crystallite contained ca. 10 layers of P3HT main chains π-stacked parallel to the substrate with their alkyl chains positioned normal to substrate at the (100) reflection, and each cluster contained ca. 39600 PCBM molecules.

To discern the surface confinement effect on thin film by electrodes,[19] we have carried out SAXS measurements on bulk P3HT/PCBM composite that have the same composition and experienced the same annealing process as that of 100 nm thin film with one-side confined on a Si substrate. In Figure 6, in the low-Q region, the SAXS profile of the annealed bulk sample carries similar features to that of the annealed thin film, with R_g of (22 ± 3) nm and (23 ± 3) nm for PCBM clusters for the bulk and the thin film case, respectively. This reveals that more than 95% accuracy for our results. We expected that the size difference in PCBM cluster between double-side confinement and one-side confinement on a 100 nm thin film should not differ more than that we have observed between the bulk and the one-side confined thin film of P3HT/PCBM. Furthermore, one report indicated the strength of substrate interactions on a polymer thin films was minimum when the film thickness is more than 17 nm, judging from the glass transition temperature.[20] Therefore, our basic conclusions on the correlation between the PCBM aggregate size and the device efficiency should be correct.

In summary, we applied GISAXS and GIWAXD simultaneously to study the morphologies of P3HT/PCBM active layers in bulk heterojunction solar cells annealed at various temperatures. This approach allowed us to investigate the effects of the sizes of the PCBM clusters and P3HT crystallites on the power conversion efficiencies of bulk heterojunction solar cells. It appears that improved power conversion efficiency requires the value of R_g of the PCBM clusters to be greater than 20 nm and the value of D_{100} of the P3HT crystallites to be greater than 16 nm for an active layer thickness of ca. 100nm.

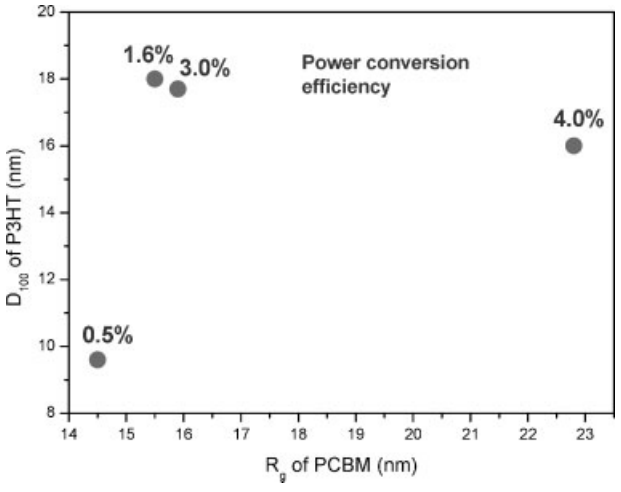

Figure 5. Relative length scales of the P3HT crystallites, the radii of gyration of the PCBM clusters, and the power conversion efficiencies of the various P3HT/PCBM film devices.

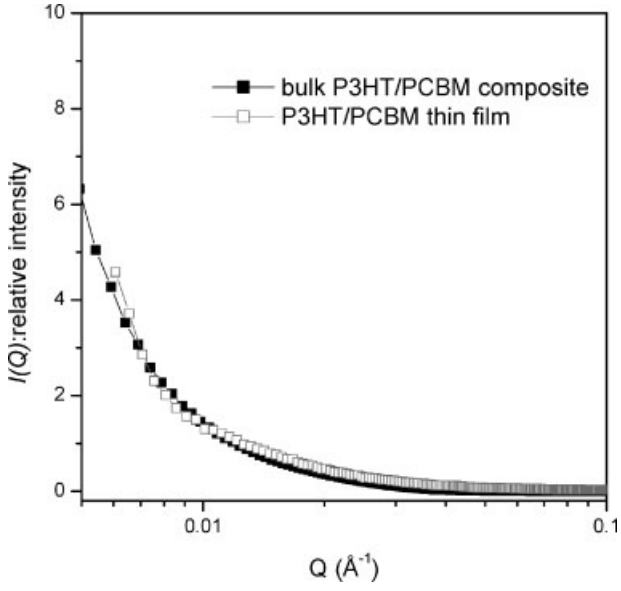

Figure 6. Comparison of the SAXS and GISAXS data for the bulk P3HT/PCBM composite and the thin film (100 nm) on a Si substrate at annealing 150 °C for 15 min.

© 2008 WILEY-VCH Verlag GmbH & Co. KGaA, Weinheim

Experimental

Device Fabrication: Regioregular poly(3-hexylthiophene) (M_w 50000 g mol^{-1}, used as received) and [6,6]-phenyl-C_{61}-butyric acid methyl ester were obtained from Rieke Metals and Nano-C Inc., respectively. P3HT was dissolved in chlorobenzene (15 mg mL^{-1}) and blended with a solution of PCBM in chlorobenzene (12 mg mL^{-1}). The P3HT/PCBM composite weight ratio was 1:0.8. The indium tin oxide (ITO)-coated glass substrate (UID Co., Ltd.; surface resistance: 15 Ω/□) was cleaned through ultrasonic treatment in detergent, methanol, acetone, and isopropyl alcohol and then it was dried in an oven overnight. PEDOT:PSS (Baytron P VP A1 4083) was spin-coated on the ultraviolet ozone-treated ITO. After annealing the PEDOT:PSS film (ca. 40 nm) at 140 °C for 30 min in air, the sample was transferred to a glove box. The P3HT/PCBM solution blend was spin-coated on top of the PEDOT:PSS layer. The thickness of film was ca. 100 nm (AFM). Finally, the Al electrode (100 nm) was deposited on the P3HT/PCBM layer under high vacuum (ca. 10^{-7} Torr (1 Torr = 1.333×10^2 Pa)) using a thermal evaporator. For thermal annealing, the completed devices were placed directly on a digitally controlled hotplate and heated at various temperatures for 15 min. After annealing, the devices were encapsulated in UV-curing epoxy and analyzed in an air atmosphere.

Calibration and Measurement: Current density–voltage characteristics of the P3HT/PCBM devices were measured under simulated AM1.5G irradiation (100 mW cm^{-2}) using a Xe lamp-based Newport 66902 150-W solar simulator. A Xe lamp equipped with an AM1.5G filter was used as the white light source. The spectrum of the solar simulator was calibrated by a PV-measurement (PVM-154) mono-Si solar cell (NREL calibrated), and Si photo diode (Hamamatsu S1133) was used to check the irradiation of the exposed area (100 mW cm^{-2}). The mismatch factor (M) was 1.34, which was obtained by taking the PVM-154 as the reference cell and our devices as the test cells and calculating the spectrum from 300 nm to 900 nm with intervals of 10 nm. The PVM-154 combined with KG-5 filter (350–700 nm passed, Newport) was to simulate a reference solar cell with spectral responsivity from 350 nm to 700 nm. The calibration was based on the IEC-69094-1 spectrum [21]. The *J–V* characteristics were measured using a Keithley 236 source measurement unit.

Characterization: Grazing-incidence small-angle X-ray scattering (GISAXS) and wide-angle X-ray diffraction (GIWAXD) measurements were performed at the SWAXS endstation of the BL17B3 beamline of the Taiwan light source at the National Synchrotron Radiation Research Center (NSRRC). The BL17B3 beamline [22], equipped with a SAXS area detector and a WAXS linear detector (in the meridian direction) connected to two data acquisition systems operated in master-slave mode, allows one to perform simultaneously SAXS/WAXS measurements for correlated changes of the crystalline structures and nanostructure of the interesting sample thin films. The wave vector transfer Q was equal to $4\pi \sin(\theta/2)/\lambda$, which was defined in terms of the scattering angle θ and wavelength λ of the X-rays. The X-rays passed through a slit having a width of 0.5 mm; the photon energy was 10.5 keV ($\lambda = 1.1809$ Å); the sample-to-detector distances were 3.2 and 0.75 m for the GISAXS and GIWAXS systems, respectively; the angle of incidence was 0.3 ° with an accuracy of 0.005 °. The samples were prepared on 3×3.5 cm^2 silicon substrates through the spin-coating of a P3HT/PCBM solution; the film thickness was the same for each sample (ca. 100 nm). X-ray diffraction measurements (Q ranging from 0.25 to 1.1 Å^{-1}) were performed using a Bede D1 high-resolution X-ray diffractometer and fixed angle of incidence (0.3 °; $\lambda = 1.54$ Å). The devices' morphologies were recorded under ambient conditions using an atomic force microscope operated in tapping-mode and a Digital Nanoscope IIIa instrument.

Received: December 13, 2007
Revised: January 11, 2008
Published online: June 2, 2008

[1] a) M. M. Wienk, J. M. Kroon, W. J. H. Verhees, J. Knol, J. C. Hummelen, P. A. Van Hal, R. A. J. Janssen, *Angew. Chem. Int. Ed.* **2003**, *42*, 3371. b) H. Hoppe, M. Niggemann, C. Winder, J. Kraut, R. Hiesgen, A. Hinsch, D. Meissner, N. S. Sariciftci, *Adv. Funct. Mater.* **2004**, *14*, 1005.

[2] a) F. Padinger, R. S. Rittberger, N. S. Sariciftci, *Adv. Funct. Mater.* **2003**, *13*, 85. b) M. Reyes-Reyes, K. Kim, D. L. Carroll, *Appl. Phys. Lett.* **2005**, *87*, 083506. c) C. N. Hoth, S. A. Choulis, P. Schilinsky, C. J. Brabec, *Adv. Mater.* **2007**, *19*, 3973.

[3] a) Y. T. Chang, S. L. Hsu, M. H. Su, K. H. Wei, *Adv. Funct. Mater.* **2007**, *17*, 3326. b) J. Peet, J. Y. Kim, N. E. Coates, W. L. Ma, D. Moses, A. J. Heeger, G. C. Bazan, *Nat. Mater.* **2007**, *6*, 497. c) F. Zhang, W. Mammo, L. M. Andersson, S. Admassie, M. R. Andersson, O. Inganäs, *Adv. Mater.* **2006**, *18*, 2169. d) D. Mühlbacher, M. Scharber, M. Morana, Z. Zhu, D. Waller, R. Gaudiana, C. Brabec, *Adv. Mater.* **2006**, *18*, 2884. e) A. M. Ballantyne, L. Chen, J. Nelson, D. D. C. Bradley, Y. Astuti, A. Maurano, C. G. Shuttle, J. R. Durrant, M. Heeney, W. Duffy, I. McCulloch, *Adv. Mater.* **2007**, *19*, 4544. f) N. Blouin, A. Michaud, M. Leclerc, *Adv. Mater.* **2007**, *19*, 2295.

[4] a) W. Ma, C. Yang, X. Gong, K. Lee, A. J. Heeger, *Adv. Funct. Mater.* **2005**, *15*, 1617. b) G. Li, V. Shrotriya, J. Huang, Y. Yao, T. Moriarty, K. Emery, Y. Yang, *Nat. Mater.* **2005**, *4*, 864. c) J. Y. Kim, S. H. Kim, H. H. Lee, K. Lee, W. Ma, X. Gong, A. J. Heeger, *Adv. Mater.* **2006**, *18*, 572. d) M. C. Scharber, D. Mühlbacher, M. Koppe, P. Denk, C. Waldauf, A. J. Heeger, C. J. Brabec, *Adv. Mater.* **2006**, *18*, 789.

[5] T. Erb, U. Zhokhavets, G. Gobsch, S. Raleva, B. Stuhn, P. Schilinsky, C. Waldauf, C. J. Brabec, *Adv. Funct. Mater.* **2005**, *15*, 1193.

[6] a) X. Yang, J. Loos, S. C. Veenstra, W. J. H. Verhees, M. M. Wienk, J. M. Kroon, M. A. J. Michels, R. A. J. Janssen, *Nano Lett.* **2005**, *5*, 579. b) W. Ma, C. Yang, A. J. Heeger, *Adv. Mater.* **2007**, *19*, 1387. c) W. Ma, A. Gopinathan, A. J. Heeger, *Adv. Mater.* **2007**, *19*, 3656. d) X. Yang, G. Lu, L. Li, E. Zhou, *Small* **2007**, *3*, 611.

[7] V. Shrotriya, Y. Yao, G. Li, Y. Yang, *Appl. Phys. Lett.* **2006**, *89*, 063505.

[8] C. R. McNeill, B. Watts, L. Thomsen, W. J. Belcher, A. L. D. Kilcoyne, N. C. Greenham, P. C. Dastoor, *Small* **2006**, *2*, 1432.

[9] a) C. P. Li, C. H. Wu, K. H. Wei, J. T. Sheu, J. Y. Huang, U. S. Jeng, K. S. Liang, *Adv. Funct. Mater.* **2007**, *17*, 2283. b) S. W. Yeh, K. H. Wei, Y. S. Sun, U. S. Jeng, K. S. Liang, *Macromolecules* **2003**, *36*, 7903.

[10] a) H. Sirringhaus, P. J. Brown, R. H. Friend, M. M. Nielsen, K. Bechgaard, B. M. W. Langeveld-Voss, A. J. H. Spiering, R. A. J. Janssen, E. W. Meijer, P. Herwig, D. M. De Leeuw, *Nature* **1999**, *401*, 685. b) T. J. Prosa, M. J. Winokur, J. Moulton, P. Smith, A. J. Heeger, *Macromolecules* **1992**, *25*, 4364. c) R. J. Kline, D. M. DeLongchamp, D. A. Fischer, E. K. Lin, L. J. Richter, M. L. Chabinyc, M. F. Toney, M. Heeney, I. McCulloch, *Macromolecules* **2007**, *40*, 7960.

[11] B. D. Cullity, *Elements of X-Ray Diffraction*, Addison-Wesley, Reading, MA **1956**.

[12] a) K. Yazawa, Y. Inoue, T. Yamamoto, N. Asakawa, *Phys. Rev. B* **2006**, *74*, 094204. b) V. Causin, C. Marega, A. Marigo, L. Valentini, J. M. Kenny, *Macromolecules* **2005**, *38*, 409.

[13] K. A. Affholter, S. J. Henderson, G. D. Wignall, G. J. Bunick, R. E. Haufler, R. N. Compton, *J. Chem. Phys.* **1993**, *99*, 9224.

[14] D. Chirvase, J. Parisi, J. C. Hummelen, V. Dyakonov, *Nanotechnology* **2004**, *15*, 1317.

[15] For general aggregate estimation using the Guinier approximation, where QR_g is less than 1, the value of Q (0.006 Å^{-1}) provided by GISAXS can be used to determine that the maximum size of R_g will be 16 nm; the sample was consistent with that obtained using bulk sample SAXS data (Q_{min}, 0.0038 Å^{-1}; maximum size of R_g, 26 nm).

[16] For a sphere, $R_g^2 = (3/5)R^2$, where R is the radius.

[17] V. D. Mihailetchi, H. Xie, B. de Boer, L. J. A. Koster, P. W. M. Blom, *Adv. Funct. Mater.* **2006**, *16*, 699.

© 2008 WILEY-VCH Verlag GmbH & Co. KGaA, Weinheim

ADVANCED MATERIALS

[18] M. M. Mandoc, W. Veurman, J. Sweelssen, M. M. Koetse, P. W. M. Blom, *Appl. Phys. Lett.* **2007**, *91*, 073518.
[19] P. Peumans, S. Uchida, S. R. Forrest, *Nature* **2003**, *425*, 158.
[20] S. Ge, Y. Pu, W. Zhang, M. Rafailovich, J. Sokolov, C. Buenviaje, R. Buckmaster, R. M. Overney, *Phys. Rev. Lett.* **2000**, *85*, 2340.
[21] V. Shrotriya, G. Li, Y. Yao, T. Moriarty, K. Emery, Y. Yang, *Adv. Funct. Mater.* **2006**, *16*, 2016.
[22] Y. H. Lai, Y. S. Sun, U. S. Jeng, J. M. Lin, T. L. Lin, H. S. Sheu, W. T. Chuang, Y. S. Huang, C. H. Hsu, M. T. Lee, H. Y. Lee, K. S. Liang, A. Gabriel, M. H. J. Koch, *J. Appl. Crystallogr.* **2006**, *39*, 871.

© 2008 WILEY-VCH Verlag GmbH & Co. KGaA, Weinheim